Dynamic Coupling for Underactuated Compliant Arms With Not Well-Defined Relative Degree

Michele Pierallini, *Member, IEEE*, Franco Angelini, *Member, IEEE*, and Manolo Garabini

***Abstract*—Soft robots are deformable, compliant, and underactuated systems. During any task, due to their enormous capability of body deformation, the relative degree may not be well-defined. Since the applicability of the large majority of the state-of-the-art control techniques depends on this property, they frequently encounter singularities. This fact can jeopardize the system's safety, prevent the correct task execution, or reduce performance. In this work, we investigate the relative degree of dependence for a class of compliant underactuated arms. Our method leverages the well-known strong inertial coupling hypothesis that, if holds, guarantees a constant relative degree of two. We generalize it by introducing coupling conditions where the relative degree is assured to be piecewise constant and greater than two. Relying on the design parameters, we analyze the dynamic evolution of the coupling conditions, which are then used to synthesize a classic input–output feedback controller. We also prove the stability of the closed-loop system. Finally, we validate the efficacy of the approach in simulation and on real hardware using a two and three degrees of freedom underactuated compliant arms with varying stiffness profiles, tasks, and disturbances.**

***Index Terms*—Flexible structures, motion control, nonlinear systems, robots.**

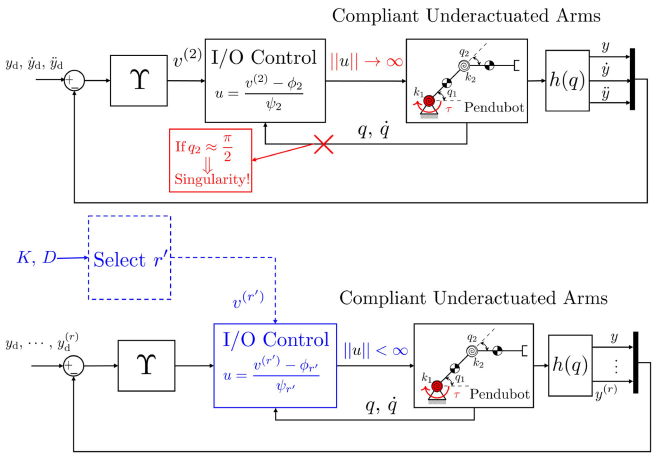

Fig. 1. Block diagrams picturing the relative degree dependence problem and the proposed approach for compliant underactuated arms, top and bottom, respectively. In red, we highlight the singularity problem for the input–output feedback linearization controller using a relative degree equal to two. In the bottom scheme, the main contribution of this article is highlighted in blue. We derive coupling conditions by selecting the robust relative degree r' leveraging the stiffness and damping matrix.

I. Introduction

SOFT robots are characterized by deformable or continuous bodies and elastic elements [1], [2]. A subclass of soft robots is the compliant underactuated arms [3]. They are designed with lightweight, e.g., [3], or deformable/continuous material, e.g., [4], and exploit novel properties, such as adaptability [5], deformability [6], and shock absorption, which are crucial to operate and interact in real-life scenarios, e.g., agri-food [7] and healthcare [8].

Despite the great effort into the fabrication of soft structures [9], [10], the modeling [11], [12], [13] and the control problems are yet to be solved [14]. Recalling the so-called control-oriented models [12] that derive from a discretization approach of the continuous beam, we focus on the control problem. The challenge, posed by the underactuation, lies in the fact that the relative degree of compliant arms is not well-defined leading to unbounded and dangerous control action. The compliant arm class, treated in this article, relies on the intersection of the two main players in the soft robot scenario: 1) continuum and 2) articulated robots [15]. They can be articulated with a generic number of passive joints [3] or continuous with lightweight materials [4].

To deal with the control of soft robots, two different approaches have been proposed. The first is a learning-based method [16], [17], [18], [19], [20], [21], [22], while the second is a classical model-based technique [14], [15], [23], [24], [25]. Both approaches are successfully exploitable if the relative degree is well defined [3], [14], [26], [27], [28]. For instance, Spong [26] proposed a condition, namely strongly inertially coupled (SIC), that guarantees a fixed relative degree. The same condition is employed in a soft continuum robot with affine curvature [29]. However, this limits the method's applicability, especially in the case of a generic number of passive joints. Therefore, what can one guarantee when the relative degree changes?

In the literature of underactuated systems control [30], [31], the effect of the relative degree dependence has been addressed but not yet solved for compliant robots. In [32], the

Manuscript received 8 March 2024; revised 8 July 2024; accepted 24 August 2024. Date of publication 9 September 2024; date of current version 20 November 2024. This work was supported in part by the European Union's Horizon 2020 Research and Innovation Programme (Natural Intelligence) under Agreement 101016970 and (DARKO) Agreement 101017274; in part by the Ministry of University and Research (MUR) as part of the PON 2014-2021 "Research and Innovation" resources—Green/Innovation Action—DM MUR under Grant 1062/2021; and in part by the Italian Ministry of Education and Research in the framework of the "FoReLab" (Future-Oriented Research Lab) Project (Departments of Excellence). This article was recommended by Associate Editor C. Yang. *(Corresponding author: Michele Pierallini.)*

The authors are with the Centro di Ricerca Enrico Piaggio and Dipartimento di Ingegneria dell'Informazione, Università di Pisa, 56126 Pisa, Italy (e-mail: michele.pierallini@gmail.com).

This article has supplementary material provided by the authors and color versions of one or more figures available at https://doi.org/10.1109/TSMC.2024.3451469.

Digital Object Identifier 10.1109/TSMC.2024.3451469

classic Feedback Linearization controller deals with multibody mechanical systems and the applicability of the method, i.e., fixed relative degree, is guaranteed by design solutions that solve the nonminimum phase problem. However, not always the robot's design can be changed. The relative degree challenge can be tackled from the control perspective. The first technique is the approximation feedback linearization (AFL) [33], [34], [35], [36], [37]. The idea is to modify the drift and/or the control vector field to achieve a well-posed canonical form and a fixed relative degree. In [37], this paradigm is applied to a compliant underactuated manipulator; however, the Authors consider a fixed relative degree equal to two and a linear output function. None of [33], [34], [35], [36], and [37] tackle the problem from a generic number of actuated joints in the chain. The second algorithm is the dynamic extension (DE) [38], [39]. The idea is to keep deriving the system's dynamics until a well-conditioned Byrnes–Isidori form is achieved. In [39] and [40], DE deals with a flexible link and joint robots respectively, while [38] tackles the control of a vessel. The third class of algorithm is the Sliding mode ones [41]. In [42] and [43], the method is experimentally applied to flexible link robots and planar n degrees of freedom (DoFs) with one passive joint, respectively. The well-definiteness of the relative degree is guaranteed thanks to the sliding policy. Other types of controllers are the Learning (also from demonstration) strategy, e.g., [17], [44], and [45], virtual input-based, and output redefinition-based dynamic inversion [38]. However, these techniques result in a substantial modification of the robot dynamics or are time-consuming. In addition, due to the complex system's dynamics and the learning paradigm, the change of the relative degree at some point of the manifold is often unknown.

This article studies the relative degree changes in a compliant underactuated arm class among any task and output function deriving controllability-like conditions. In particular, this article's main contribution is the study of the relative degree of dependence for control purposes of compliant underactuated robots and, for the first time, we link it to the compliant robot's dynamics with the following steps.

This article studies the relative degree changes in a compliant underactuated arm class among any task and output function deriving controllability-like conditions. In particular, this article's main contribution is the study of the changes of the relative degree for control purposes in compliant underactuated robots and, for the first time, we link it to the compliant robot's dynamics with the following steps.

1) We derive new coupling dynamic conditions generalizing the SIC one [26] by taking into account high-order derivatives of both the (freely chosen) output function and the underactuated robot dynamics.
2) We study the relationship between the compliant underactuated robots' dynamic and high-order terms w.r.t. design choices.
3) We use a classic model-based output feedback controller, i.e., AFL [36], proving the reliability of both the new conditions (1) and the high-order dynamic terms evolution (2). As a minor contribution, we prove the stability of the closed-loop system using (1) and (2).

Points (1)–(3) are theoretical and represent the contribution of this article. The method's effectiveness is tested in simulations and on real hardware. We simulate a three-DoF lightweight robot and a continuum one. Experiments use a two-DoF lightweight robot. Only the first state is active in all the arms, and we vary the stiffness profile, task, relative degree, and disturbances. Moreover, we compare the performance with standard controllers applicable to underactuated systems.

Notation: Let 0_n, $I_n \in \mathbb{R}^{n\times n}$ be the zero and the identity matrix, respectively. For any matrix $A \in \mathbb{R}^{n\times m}$, the symbol A_{ij} indicates its (i,j)th element and, let $q(t) : [0,\ t] \to \mathbb{R}^n$, we define $\nabla_q A(q)\dot{q} \triangleq \sum_{i=1}^{n} \nabla_{q_i} A(q)\dot{q}_i$. The symbol $\|(\cdot)\|$ indicates the $\|(\cdot)\|_1$. Let be $f(\cdot), g(\cdot) : \mathbb{R}^n \to \mathbb{R}^n$, $L_f g(x)$ stands for the Lie derivative and $ad_f g(x)$ indicates the Lie brackets, i.e., $ad_f g(x) = L_f g(x) - L_g f(x) = (\partial g(x)/\partial x)\ f(x) - (\partial f(x)/\partial x)\ g(x) = \nabla_x g(x) f(x) - \nabla_x f(x) g(x)$. For any function $f(\cdot) : \mathbb{R}^n \times [0, t_f] \to \mathbb{R}^n$, the symbol $f^{(i)}(x(t))$ indicates its ith time derivative. $O(\cdot)$ indicates the approximation order of $(\cdot)$. Finally, $\mathscr{D}_{(\cdot)}$ indicates any compact set of $(\cdot)$.

II. Problem Definition

We refer to the model of a compliant underactuated arm [3] modeled using lumped parameters (LP) [3] and a piecewise constant curvature (PCC) description [4], which combines one actuated state and a generic number of unactuated ones, i.e.,

$$M(q)\ddot{q} + \chi(q,\dot{q}) + G(q) + D\dot{q} + Kq = Fu \tag{1}$$

where $q,\ \dot{q},\ \ddot{q} \in \mathscr{D}_q \subset \mathbb{R}^n$ are the Lagrangian variables position, velocity and acceleration vectors, respectively. $M(q) \in \mathbb{R}^{n\times n}$ is the symmetric inertia matrix, such as $M(q) \succ 0\ \ \forall q \in \mathscr{D}_q$. $\chi(q,\dot{q}) \in \mathbb{R}^n$ and $G(q) \in \mathbb{R}^n$ are the Coriolis and gravity vector, respectively. $D \in \mathbb{R}^{n\times n}$ and $K \in \mathbb{R}^{n\times n}$ are the damping and spring matrix, such as $K,\ D \succ 0$ and $||K|| > 1$. $u \in \mathbb{R}$ is the control input, and $F \in \mathbb{R}^n$ is the underactuation matrix, i.e., $\text{rank}\{F\} = 1$, hence the number of the passive state is $n-1$.

The dynamics model (1) describes a great variety of compliant underactuated arms. In this article, we will validate our method using an LP [3] and a PCC model [4], [46], [47]. LP usually describes lightweight flexible link robots, while PCC refers to soft continuous robots, and both robots belong to the complaint underactuated arms class described in (1).

Let $\mathscr{D}_x \subset \mathbb{R}^{2n}$ be a compact set, and let $x \triangleq [q^\top,\ \dot{q}^\top]^\top \in \mathscr{D}_x$ be the state of the system, we can rearrange (1) in the affine state-space form representation, i.e.,

$$\begin{cases} \dot{x}(t) = f(x(t)) + g(x(t))u(t) & (2) \\ y(t) = h(x(t)) & (3) \end{cases}$$

where $x_0 \triangleq x(0)$ is the initial condition, $t \in [0, t_f]$ is the time variable, $f(\cdot) : \mathscr{D}_x \times [0, t_f] \to \mathbb{R}^{2n}$ with $f(x_0) = 0_{2n\times 1}$ and $g(\cdot) : \mathscr{D}_x \times [0, t_f] \to \mathbb{R}^{2n}$ are the drift and control vector field, respectively, i.e.,

$$f(x) = \begin{bmatrix} \dot{q} \\ -M^{-1}(q)N(q,\dot{q}) \end{bmatrix},\ \ g(x) = \begin{bmatrix} 0_{n\times 1} \\ M^{-1}(q)F \end{bmatrix} \tag{4}$$

with $N(q,\dot{q}) \triangleq \chi(q,\dot{q}) + G(q) + Kq + D\dot{q}$. $y \in \mathbb{R}$ is the output of the system, and $h(\cdot) : \mathscr{D}_x \times [0, t_f] \to \mathbb{R}$ is the output function.

The system (2) and (3) has a not well-defined relative degree r within the task. This means that it varies for some $t \in [0, t_f]$, and $x \in \mathscr{D}_x$ (e.g., [48]). In addition, let us indicate with r' the robust relative degree (e.g., [34]). Note that it holds $r' \geq r$ [34]. Now, let us assume what follows.

Assumption 1: Recalling (2) and (3), $f(\cdot)$, $g(\cdot)$, $h(\cdot)$, $L_f^k h(\cdot)$, and $L_g L_f^{k-1} h(\cdot)$ for $k = 1, \ldots, 2n$ are locally Lipschitz with constant f_0, g_0, h_0, $L_f^k h_0$, $L_g L_f^{k-1} h_0$, i.e., $||f(x_1) - f(x_2)|| \leq f_0 ||x_1 - x_2|| \quad \forall x_1, x_2 \in \mathscr{D}_x$.

Assumption 1 is a classic one. Recalling [49] and (1), there exist constants, such as $\mu_{\mathrm{m}} \leq ||M(q)|| \leq \mu_{\mathrm{M}}$, $||\chi(q, \dot{q})|| \leq \mu_{\mathrm{C}}(\|\dot{q}\| + \|q\|)$, and $||G(q)|| \leq \mu_{\mathrm{G}} \|q\|$. Hence, one has that $f_0 = \mu_m^{-1}(\mu_C + \mu_{\mathrm{G}} + ||K|| + ||D||)$. Since μ_m, $\mu_C \ll 1$, $\mu_G \approx 1$, and $||K|| > 1$, then it holds that $f_0 > 1$. Note that f_0 depends on the system's physical design, material, and geometry of the robot. Moreover, it hold that $g_0 = \mu_{\mathrm{m}}^{-1} > 0$, and $h_0 > 0$.

Assumption 2: The output function $y(\cdot) : [0, t_f] \times \mathscr{D}_x \to \mathbb{R}$ in (3) is $C^{r'}([0, t_f])$ and it can be written as a (nonlinear) combination of the joint positions, i.e.,

$$y = h(x(t)) = h(q(t)) \ . \tag{5}$$

Moreover, we assume that $\nabla_q^{(l)} h(q)|_{\overline{q}} \neq 0_{1 \times n}$, for $l = r, \ldots, r'$ and almost all $\overline{q} \in \mathscr{D}_q$.

We highlight that output functions in the form of (6) are very common in robotics. An example is a combination of the joint [3] or the Cartesian coordinates of the robot end-effector [14], which are smooth functions belonging to $C^{r'}[0, t_f]$.

Assumption 3: For (2), the controllability condition holds true for $x_0 \in \mathscr{D}_x$, i.e., $\mathrm{rank}\{g, ad_f g, , \ldots, ad_f^{2n-1} g\}(x_0) = 2n$. Assumption 3 is a controllability condition, which guarantees the existence of a control action from an equilibrium x_0 to a certain state x_f in finite time, i.e., t_f. However, it is well known that the compliant underactuated arms in (1) are small-time locally controllable [50], [51], [52], but they do not satisfy the necessary condition to be fully linearized via input to the state controller, i.e., $\mathrm{rank}\{g, ad_f^2 g\}(\bar{x}) < \mathrm{rank}\{g, ad_f g\}(\bar{x})$ for some $\bar{x} \in \mathscr{D}_x$, see [34], [36], [53]. In other words, a controller, that moves the system up to a certain state in finite time, exists, but it cannot be designed in an input-to-output fashion. Therefore, one can proceed by approximating the system (2) and (3) with one being input-to-state linearizable, and it would be possible to design the controller [36].

Finally, the goals of this work are the following.

Goal 1: Generalization of the SIC condition [26] by developing controllability conditions, which ensure dynamic coupling between the active and passive joints for (1) and (5).

Goal 2: Analyze the high-order dynamic terms evolution in (1) and (5) highlighting the role of stiffness and damping terms.

Goal 3: Let $y_d(t) : [0, t_f] \to \mathbb{R}$ be the desired output function which is $C^{r'}([0, t_f])$. Use a classic model-based feedback controller relying on G1 and G2 to guarantee the stable tracking of $y_d(t)$ with $t_f < +\infty$.

In the following two sections, we aim to exploit the compliant underactuated arm dynamics in two ways. First, we derive dynamic conditions to guarantee a coupling between the active and unactuated joints in (1), (2), and (5) (Section III). Second, we propose a control law, which solves the trajectory tracking problem with a bounded error (Section IV).

III. On the Relative Degree of Compliant Underactuated Arms

In this section, differentiating the arbitrarily chosen output function (5), we derive a local diffeomorphism to approximate the system (2)–(5) and transform it into one written in canonical form. Then, we propose dynamic conditions generalizing the well-known SIC one in [26]. Finally, we highlight the contribution of the physical parameters, such as stiffness and damping term in (1) in the relative degree variation.

A. Motivational Example

Classic model-based controllers assume that the relative degree r of the system is fixed along the desired task. This is sufficient to guarantee the boundedness of the control input [3], [15], [26]. However, when the robot is soft or underactuated, the relative degree is not well-defined among the whole manifold and the naive use of model-based feedback controllers close these singularities leads to unbounded control action. A clear example is the pendubot, i.e., two DoFs arm [26] also in the case of elastic joints [3]. Let $q = [q_1, q_2]^\top \in \mathbb{R}^2$ be the configuration and let $y = q_1 + q_2$ be the output function. Then, the relative degree is equal to $r = 2$ iff $L_g L_f h(q) = b_2 \cos(q_2)/\mathrm{detM}(q) \neq 0 \quad \forall q \in \mathbb{R}^2$, where $b_2 \in \mathbb{R}$ is an inertial parameter and $\mathrm{detM}(q) \neq 0 \quad \forall q \in \mathbb{R}^2$. Clearly, $L_g L_f h(q)$ vanishes when the relative position of the second joint, i.e., q_2, is $q_2 = \pi/2$. Therefore, the classic feedback linearization control law [48], i.e., $u(t) = (v - L_f^2 h(x))/L_g L_f h(x)$ where v is an additional control input to be selected, becomes unbounded when $q_2 \to \pi/2$. It is worth mentioning that this is a robot inertial property, and that q_2 approaches $\pi/2$ more frequently while decreasing the robot stiffness. In Section V-A, we will report the simulation showing this peculiarity.

Considering a PCC model [4], selecting, as output function (5), the orientation of the robot's tip. The problem of relative degree affects the PCC model in the vertical configuration, where $L_g L_f h(x) \to 0$ leads to unbounded control action. Please refer to Section V-A for further details.

B. Derive Approximated Diffeomorphism

We determine a diffeomorphism w.r.t. the relative degree.

Let us suppose that, the system (2)–(6) has relative degree r for some $x \in \mathscr{D}_x$, i.e., $y^{(r)} = L_f^r h(x) - L_g L_f^{r-1} h(x(t))u$. However, for some other $x \in \mathscr{D}_x$, it holds that $|L_g L_f^{r-1} h(x(t))| \approx 0$. Thus, model-based input–output controllers become divergent (e.g., [48]) but, in general, no control action can affect the output's evolution, i.e., loss of controllability. To avoid this, one can keep differentiating the output function (6), gaining new coupling conditions to design a well-defined new control action.

Differentiating the output function (3) w.r.t. time, one has

$$\begin{cases} y = h(x) = \phi_0(x) \\ \quad \cdots \\ y^{(r)} = L_f^r h(x) + L_g L_f^{r-1} h(x) u = \phi_r(x) + \psi_r(x) u \\ y^{(r+1)} = \phi_{r+1}(x) + \psi_{r+1}(x) u + \theta_{r+1}\left(x, u^2\right) + \omega_{r+1}(x, \dot{u}) \\ \quad \cdots \\ y^{(r')} = \phi_{r'}(x) + \psi_{r'}(x) u + \theta_{r'}\left(x, u^2, \ldots, u^{r'-r+1}\right) \\ +\omega_{r'}\left(x, u, u^2, \ldots, u^{r'-r}, \dot{u}, \ldots, u^{(r'-r+1)}\right) \end{cases} \tag{6}$$

where $\phi_0(x) \triangleq h(x)$, and for $k = 1, \ldots, r'$, we have

$$\begin{aligned} \phi_k(x) &= \nabla_x \phi_{k-1}(x) f(x) \\ &= \nabla_q \phi_{k-1}(x) \dot{q} - \nabla_{\dot{q}} \phi_{k-1}(x) M^{-1}(q) N(q, \dot{q}). \end{aligned} \tag{7}$$

The terms $\psi_i(x)$ represent the affine terms in the control action in (6). They are computed such that $\psi_i(x) = 0$ for $i = 0, \ldots, r-1$, while for $i = r, \ldots, r'$, one has

$$\begin{aligned} \psi_i(x) &= \nabla_x \psi_{i-1}(x) f(x) + \nabla_x \phi_{i-1}(x) g(x) \\ &= \nabla_q \psi_{i-1}(x) \dot{q} - \nabla_{\dot{q}} \psi_{i-1}(x) M^{-1}(q) N(q, \dot{q}) \\ &\quad + \nabla_{\dot{q}} \phi_{i-1}(x) M^{-1}(q) F. \end{aligned} \tag{8}$$

Analogously, the terms $\theta_j(x, \cdot)$ in (6) are such that $\theta_j(\cdot) = 0$ for $j = 0, \ldots, r$, while for $j = r+1, \ldots, r'$, one has

$$\begin{aligned} \theta_j(x, u^2, \ldots, u^{j-r+1}) &= \nabla_x \psi_{j-1}(x) u g(x) u \\ &\quad + \theta_{j-1}(x, u^2, \ldots, u^{j-r})(f(x) + g(x)u). \end{aligned} \tag{9}$$

Finally, the terms $\omega_j(\cdot)$ group the time derivatives of the control action derived by the control input powers in $\theta_{j-1}(\cdot)$ and $\psi_i(x)$ for $i = r, \ldots, r'$, i.e., $\omega_j(\cdot) = 0$ for $j = 0, \ldots, r$ while for $j = r+1, \ldots, r'$, one has

$$\omega_j(x, \cdot) = \psi_{j-1}(x) \dot{u} + \frac{d}{dt} \frac{\partial}{\partial u} \theta_{j-1}(x, \cdot) + \frac{d\omega_{j-1}(x, \cdot)}{dt}. \tag{10}$$

In the following, we often refer to $\phi_k(\cdot)$, $\psi_i(x)$, and $\omega_j(\cdot) = 0$ for $k, i, j = r, \ldots, r'$ as high order terms of the system (2)–(5).

Assumption 4: The functions $\omega_j(x, \cdot)$ for $j = r+1, \ldots, r'$ in (6) are $O(x)$, i.e., $\lim_{t \to t_f} |\omega_j(x(t), \cdot)| / \|x(t)\| = 0$.

Assumption 4 is reasonable thanks to Assumptions 1 and 3. From a practical perspective, this means that a smooth control action exists whose derivatives are almost null and multiplied from an even small value.

Recalling the system (2), (6), and (6), we assume the existence of nonlinear local diffeomorphism $\Phi(\cdot) : \mathscr{D}_x \to \mathscr{D}_z \subset \mathbb{R}^{2n}$, such as $\det\{\nabla_x \Phi(x)\} \neq 0 \ \ \forall x \in \mathscr{D}_x$ e.g., [34] and [36]. Note that this implies that the diffeomorphism does not change during the task preserving the dynamics of the robots and it preserves the manifold's dimension. Recalling Assumption 4, we neglect $\omega_j(\cdot)$ for $j = r+1, \ldots, r'$, and define the new coordinates $z \triangleq \Phi(x) = [\xi^\top, \eta^\top]^\top = [\xi_0, \ldots, \xi_{r'-1}, \eta_0, \ldots, \eta_{2n-r'-1}]^\top \in \mathscr{D}_z \subset \mathbb{R}^{2n}$ with $\xi \in \mathscr{D}_\xi \subset \mathbb{R}^{r'}$ and $\eta \in \mathscr{D}_\eta \subset \mathbb{R}^{2n-r'}$. We set $\xi_i = \phi_i(x)$, $i = 0, \ldots, r'-1$ and select $\eta_j = \eta_j(x)$, $j = 0, \ldots, 2n-r'-1$ to guarantee $\operatorname{rank}\{\nabla_x \Phi(x)\} = 2n \ \ \forall x \in \mathscr{D}_x$. Hence, the system (2) and (3) becomes

$$\begin{cases} \dot{\xi} = A\xi + \Psi(\xi, \eta) u + \Theta\left(\xi, \eta, u^2, \ldots, u^{r'-r+1}\right) \\ \dot{\eta} = p(\xi, \eta, u) \\ y_\xi = \left[1, \ 0_{2n-1\times 1}^\top\right] \xi \triangleq C_\xi z \end{cases} \tag{11}$$

where $A_{i_a, j_a} = 0 \ \ \forall i_a, j_a = 1, \ldots, r'$, if $i_a = j_a - 1$ then $A_{i_a j_a} = 1$, $\Psi(\cdot) : \mathscr{D}_z \to \mathbb{R}^{r'}$ collecting $\psi_i(x)$ for $i = r, \ldots, r'$, $\Theta(\cdot) : \mathscr{D}_z \times \mathbb{R} \times \cdots \times \mathbb{R} \to \mathbb{R}^{r'}$ stacking $\theta_j(\cdot)$ for $j = r+1, \ldots, r'$, and $p(\cdot) : \mathscr{D}_z \times \mathbb{R} \to \mathbb{R}^{2n-r'}$. The robust relative degree r' affects the dimension of the zero-dynamics $\dot{\eta} = p(\eta, \xi, u)$ in (11) [54], [55].

C. Dynamic Coupling Conditions

In this section, we aim to solve G1. To this end, we derive dynamic conditions between the active and passive joints. Recalling (1) and differentiating the output function (6), we define controllability conditions highlighting the damping and stiffness contributions. We show that there exists a design choice to ensure a certain condition to be true $\forall x \in \mathscr{D}_x$.

Let us twice differentiate the output function (6) w.r.t. time, then we introduce the following definition.

Definition 1: The system (1)–(3) is said to be SIC (SIC=SC^2) iff $\operatorname{rank}\{\psi_2(x)\} = 1$, where

$$\psi_2(x) = L_g L_f h(x) = \nabla_q h(q) M^{-1}(q) F \,. \tag{12}$$

It is worth noting that when (12) is not fulfilled, controllers, such as partial feedback linearization (e.g., [26]), encounter singularities.

Recalling (6), one can keep differentiating the output function w.r.t. time. This leads to the following definition.

Definition 2: The system in (1)–(3) is said to be Strongly Coupled^3 (SC^3) iff $\operatorname{rank}\{\psi_3(x)\} = 1$, where

$$\begin{aligned} \psi_3(x) = &\left[3\nabla_q^2 h(q)\dot{q} - \nabla_q h(q) M^{-1}(q)\left(\nabla_{\dot{q}} \chi(q, \dot{q}) + D\right)\right] \\ &\times M^{-1}(q) F + \nabla_q h(q)\left(\nabla_q M^{-1}(q)\dot{q}\right) M^{-1}(q) F \,. \end{aligned} \tag{13}$$

Similarly, we compute the fourth output derivative w.r.t. time, and we define what follows.

Definition 3: The system (1)–(3) is said to be Strongly Coupled^4 (SC^4) iff $\operatorname{rank}\{\psi_4(x)\} = 1$, where

$$\begin{aligned} \psi_4(x) = &\nabla_q \Big[3\nabla_q^2 h(q)\dot{q} - \nabla_q h(q) M^{-1}(q)\left(\nabla_{\dot{q}} \chi(q, \dot{q}) + D\right) \\ &\times M^{-1}(q) F + \nabla_q h(q)\left(\nabla_q M^{-1}(q)\dot{q}\right) M^{-1}(q) F\Big]\dot{q} \\ &- \Big[3\nabla_q^2 h(q) M^{-1}(q) F - \nabla_q h(q) M^{-1}(q) \nabla_{\dot{q}}^2 \chi(q, \dot{q}) M^{-1}(q) F \\ &+ \nabla_q h(q) \nabla_q M^{-1}(q) F\Big] M^{-1}(q) N(q, \dot{q}, K) \\ &- \Big[3\nabla_q^3 h(q)\dot{q}^2 - \nabla_q\left(\nabla_q h(q) M^{-1}(q)\left(\nabla_{\dot{q}} \chi(q, \dot{q}) + D\right)\right)\dot{q} \\ &- \nabla_q\left(\nabla_q h(q) M^{-1}(q) N(q, \dot{q}, K)\right) - \Big[2\nabla_q^2 h(q)\dot{q} - \nabla_q h(q) \\ &\times M^{-1}(q)\left(\nabla_{\dot{q}} \chi(q, \dot{q}) + D\right)\Big] M^{-1}(q)\left(\nabla_{\dot{q}} \chi(q, \dot{q}) + D\right) - \\ &\Big[2\nabla_q^2 h(q)\dot{q} - \nabla_q h(q) M^{-1}(q) \nabla_{\dot{q}}^2 \chi(q, \dot{q})\Big] M^{-1}(q) N(q, \dot{q}, K)\Big] \\ &\times M^{-1}(q) F \,. \end{aligned} \tag{14}$$

Remark 1: The condition (12) depends on the output function (6) and inertial property of the system (1) and (2). In addition, (13) depends also on the damping matrix and joint velocities, and (14) is also a function of the stiffness of the system.

Finally, recalling (6)–(9), one can state what follows.

Definition 4: The system (2) and (3) is said to be Strongly Coupled$^{r'}$ (SC$^{r'}$) iff rank$\{\psi_{r'}(x)\} = 1$.

D. On the Stiffness and Damping Influence in the Relative Degree Variation

We study how the system's relative degree is affected by the system's physical properties, e.g., stiffness and damping. This introduces a novel element in the study w.r.t. [26], [35].

Proposition 1: Let us consider the system (1), the output function (6) and Assumption 2. There exists a design choice to guarantee the system to be SC^i for $i = 3, \dots, 2n$ $\tilde{\forall}$.[1] $x \in \mathscr{D}_x$.

Proof: To achieve the proof, we show that there exists a design choice that makes the terms $\psi_i(\cdot) : \mathscr{D}_x \to \mathbb{R}$ in (6), such as $\psi_i(x) \neq 0 \ \ \tilde{\forall} x \in \mathscr{D}_x$ with $i = 3, \dots, 2n$.

Let us analyze the time derivatives of the output function (6), i.e., (6), inductively. Recalling (1), (13), i.e., $r = 3$, and Assumption 2, the term $\psi_3(x) = \nabla_q h(q) M^{-1}(q) D M^{-1}(q) F \neq 0 \ \tilde{\forall} x \in \mathscr{D}_x$. $\psi_3(x)$ depends linearly on the damping matrix D.

Similarly, recalling (14), i.e., $r = 4$, it holds that both the terms $\psi_4(x) = \nabla_q h(q) M^{-1}(q) K M^{-1}(q) F \neq 0$ and $\nabla_q h(q) M^{-1}(q) D M^{-1}(q) D M^{-1}(q) F \neq 0 \ \ \tilde{\forall} x \in \mathscr{D}_x$. $\psi_4(x)$ depends linearly on K and quadratically on D.

Iteratively, one can use (8) noting that the term linear in K and D are present in $\psi_i(x)$ for $i = 4, \dots, 2n$. Therefore, the thesis follows. ∎

It is worth mentioning that the design of the damping matrix is typically more complex w.r.t. the stiffness one. In addition, D is usually such that $\|D\| \approx 0$, thus (13) could fail for some $x \in \mathscr{D}_x$. Hence, one can design the stiffness to guarantee (14).

The relative degree does not affect the performances in the case of a rigid link, i.e., $K_{mm} \to +\infty \ \ \forall m = 1, \dots, n$. This is an intuitive way to understand the claim of Proposition 1.

Proposition 2: Let us consider the system (1), (2), and output function (6). Let ${}^jB({}^j\bar{x}) \subset \mathscr{D}_x$ be, such as ${}^jB({}^j\bar{x}) = \{{}^j\bar{x} = [{}^j\bar{q}^\top, 0^\top_{n\times 1}]^\top \in \mathscr{D}_x \,|\, |\psi_j({}^j\bar{x})| = 0\}$ with $j = r, \dots, r'$.

Then, it exists a design choice such that ${}^jB({}^j\bar{x}) \cap {}^{j+1}B({}^{j+1}\bar{x}) = \emptyset \ \ \forall j = r, \dots, r' - 1$.

Proof: Let us proceed by induction on the differentiation order of the output and let s be the inductive index.

$s = r = 2$ leads to $\psi_2(x)$ in (12), and $\psi_2({}^2\bar{x}) = 0$.

$s = r + 1 = 3$ leads to $\psi_3(x)$ in (13), such that $\psi_3({}^2\bar{x}) = -\nabla_q h(q) \,|_{{}^2\bar{q}} \, M^{-1}({}^2\bar{q}) D M^{-1}({}^2\bar{q}) F \neq 0 \ \ \forall {}^2\bar{x} \in {}^2B({}^2\bar{x})$, thanks to the presence of the damping matrix, i.e., Proposition 1.

Let be the inductive hypothesis true. Note that this guarantees that ${}^{r'-2}B({}^{r'-2}\bar{x}) \cap {}^{r'-1}B({}^{r'-1}\bar{x}) = \emptyset$. Therefore, it holds that $\psi_{r'-2}({}^{r'-1}\bar{x}) \neq 0 \ \ \forall {}^{r'-1}\bar{x} \in {}^{r'-1}B({}^{r'-1}\bar{x})$.

[1]Note that the expression $\tilde{\forall} \triangleq$ *for almost all* derives from the output function (3) and Assumption 2.

$s = r' - 1$, recalling (8), leads to $\psi_{r'-1}(x) = \nabla_q \psi_{r'-2}(x)\dot{q} + \nabla_{\dot{q}} \phi_{r'-2}(x) M^{-1}(q) F - \nabla_{\dot{q}} \psi_{r'-2}(x) M^{-1}(q) N(q, \dot{q})$, and, substituting $\tilde{x} \triangleq {}^{r'-1}\bar{x}$, it holds that

$$\psi_{r'-1}(\tilde{x}) = \nabla_{\dot{q}} \phi_{r'-2}(\tilde{x})\Big|_{\tilde{x}} M^{-1}(\tilde{q}) F - \nabla_{\dot{q}} \psi_{r'-2}(x)\Big|_{\tilde{x}} \times M^{-1}(\tilde{q})(G(\tilde{q}) + K\tilde{q}) = 0. \tag{15}$$

Then, two solutions exist for (15), namely:

(A) if both $\nabla_{\dot{q}} \psi_{r'-2}(x)|_{\tilde{x}} = 0_{1\times n}$ and $\nabla_{\dot{q}} \phi_{r'-2}(x)|_{\tilde{x}} = 0_{1\times n}$ and

(B) If for $\tilde{x} \in {}^{r'-1}B(\tilde{x})$ it holds that

$$\nabla_{\dot{q}} \phi_{r'-2}(x)\Big|_{\tilde{x}} M^{-1}(\tilde{q}) F = \nabla_{\dot{q}} \psi_{r'-2}(x)\Big|_{\tilde{x}} M^{-1}(\tilde{q})(G(\tilde{q}) + K\tilde{q}). \tag{16}$$

Therefore, let us consider $s = r'$, the objective is to show that $\psi_{r'}(\tilde{x}) \neq 0 \ \ \forall \tilde{x} \in {}^{r'-1}B(\tilde{x})$, which leads to ${}^{r'-1}B(\tilde{x}) \cap {}^{r'}B({}^{r'}\bar{x}) = \emptyset$. Recalling (7) and (8), one has

$$\begin{aligned}
\psi_{r'}(x) = {} & \nabla_q \psi_{r'-1}(x)\dot{q} + \big[\nabla_q\big(\nabla_q \psi_{r'-3}(x)\dot{q} - \nabla_{\dot{q}} \psi_{r'-3}(x) \\
& \times M^{-1}(q) N(q, \dot{q})\big) - \nabla_{\dot{q}} \nabla_q \psi_{r'-2}\dot{q} \\
& - \nabla_{\dot{q}} \nabla_{\dot{q}} \psi_{r'-2} M^{-1}(q) N(q, \dot{q}) \\
& - \nabla_{\dot{q}}\Big(\nabla_q \psi_{r'-3}(x)\dot{q} - \nabla_{\dot{q}} \psi_{r'-3}(x) M^{-1}(q) N(q, \dot{q})\Big) M^{-1}(q) \\
& \times \big(\nabla_{\dot{q}} \chi(q, \dot{q}) + D\big)\big] M^{-1}(q) F - \big[\nabla_{\dot{q}} \nabla_q \psi_{r'-1}(x)\dot{q} \\
& + \nabla_{\dot{q}} \nabla_{\dot{q}} \phi_{r'-2}(x) M^{-1}(q) F - \nabla_{\dot{q}} \nabla_{\dot{q}} \psi_{r'-2}(x) M^{-1}(q) N(q, \dot{q}) \\
& \nabla_q\Big(\nabla_q \psi_{r'-3}(x)\dot{q} + \nabla_{\dot{q}} \phi_{r'-3}(x) M^{-1}(q) F - \nabla_{\dot{q}} \phi_{r'-3}(x) \\
& \times M^{-1}(q) N(q, \dot{q})\Big) - \nabla_q\Big(\nabla_q \psi_{r'-3}(x)\dot{q} + \nabla_{\dot{q}} \phi_{r'-3}(x) M^{-1}(q) \\
& \times F - \nabla_{\dot{q}} \phi_{r'-3}(x) M^{-1}(q) N(q, \dot{q})\Big) M^{-1}(q)\big(\nabla_{\dot{q}} \chi(q, \dot{q}) + D\big)\Big] \\
& \times M^{-1}(q) N(q, \dot{q}).
\end{aligned} \tag{17}$$

We here analyze the solution (A).

1) Case A: Recalling (17) and evaluating it in $\tilde{x}$ yield

$$\begin{aligned}
\psi^{A)}_{r'}(\tilde{x}) = {} & \nabla_{\dot{q}} \psi_{r'-3}(x)\Big|_{\tilde{x}} M^{-1}(\tilde{q}) F M^{-1}(\tilde{q}) F \\
& - \nabla_q \nabla_{\dot{q}}\big(\psi_{r'-3}(x) + \phi_{r'-3}(x)\big)\Big|_{\tilde{x}} M^{-1}(q) \\
& \times (K\tilde{q} + G(\tilde{q})) M^{-1}(\tilde{q}) F - \nabla_{\dot{q}}\big(\psi_{r'-3}(x) + \phi_{r'-3}(x)\big)\Big|_{\tilde{x}} \\
& \times M^{-1}(q)\big(K\tilde{q} + G(\tilde{q}) + K + \nabla_q G(q)\big|_{\tilde{x}}\big) M^{-1}(\tilde{q}) F \\
& + \nabla_{\dot{q}} \nabla_{\dot{q}} \psi_{r'-2}(x)\Big|_{\tilde{x}} M^{-1}(\tilde{q})(K\tilde{q} + G(\tilde{q})) M^{-1}(\tilde{q})(K\tilde{q} + G(\tilde{q})) \\
& - \nabla_{\dot{q}} \nabla_{\dot{q}} \phi_{r'-2}(x)\Big|_{\tilde{x}} M^{-1}(\tilde{q})(K\tilde{q} + G(\tilde{q})) M^{-1}(\tilde{q}) F \,.
\end{aligned}$$

Thanks to the inductive hypothesis, $\nabla_{\dot{q}} \psi_{r'-3}(x)$ and $\nabla_{\dot{q}} \phi_{r'-3}(x)$ in $\tilde{x}$ are not null, while $\nabla_q \nabla_{\dot{q}} \psi_{r'-3}(x)$ and $\nabla_q \nabla_{\dot{q}} \phi_{r'-3}(x)$ are such that $\nabla_q \nabla_{\dot{q}} \psi_{r'-3}(x) \approx \nabla_q \nabla_{\dot{q}} \phi_{r'-3}(x) \approx 0_{1\times n}$. Similarly, one has $\nabla_{\dot{q}} \nabla_{\dot{q}} \phi_{r'-2}(x) \approx \nabla_{\dot{q}} \nabla_{\dot{q}} \phi_{r'-2}(x) \approx 0_{1\times n}$. Therefore, the stiffness matrix K can be properly selected to gain $\psi^{A)}_{r'}(\tilde{x}) \neq 0$.

We here analyze the solution (B).

2) Case B: Recalling (16) and (17), one has

$$\begin{aligned}
\psi^{B)}_{r'}(\tilde{x}) = {} & -\nabla_q \phi_{r'-3}(x)\Big|_{\tilde{x}} M^{-1}(\tilde{q}) F - \nabla_{\dot{q}} \phi_{r'-3}(x)\Big|_{\tilde{x}} M^{-1}(\tilde{q}) \\
& \times D M^{-1}(\tilde{q}) D - \Big[\nabla_{\dot{q}} \phi_{r'-3}(x)\Big|_{\tilde{q}} \nabla_q M^{-1}(q)\Big|_{\tilde{q}} F - \nabla_{\dot{q}} \psi_{r'-3}(x)\Big|_{\tilde{x}}
\end{aligned}$$

$$\times M^{-1}(\tilde{q})\left(\nabla_q G(q)\Big|_{\tilde{q}} + K\right) + \nabla_{\dot{q}}\psi_{r'-3}(x)\Big|_{\tilde{x}} M^{-1}(\tilde{q})$$
$$\times DM^{-1}(\tilde{q})D - \nabla_{\dot{q}}\psi_{r'-3}(x)\Big|_{\tilde{x}} M^{-1}(\tilde{q})D\Big]M^{-1}(\tilde{q})(K\tilde{q} + G(\tilde{q})).$$

Similarly to the case A, we can conclude that $\psi_{r'}^{B)}(\tilde{x}) \neq 0 \ \forall \tilde{x} \in {}^{r'-1}B(\tilde{x}) \subset \mathscr{D}_x$, and the proof is completed. ∎

Proposition 2 states that if the system is not SC^j for some $x \in \mathscr{D}_x$, it is $SC^{j+1} \ \forall j = r, \ldots, r'-1$. This achieves G1.

IV. Control Design

In this section, we investigate the properties of compliant underactuated arms to tackle the control problem properly. Recalling (6) and Assumption 4, we analyze the dynamic evolution of the high-order terms, namely $\phi_k(\cdot)$ for $k = 0, \ldots, r'$, $\psi_i(\cdot)$ for $i = r, \ldots, r'$ and $\theta_j(\cdot)$ for $j = r+1, \ldots, r'$. Then, we use a classic controller, which copes with the high-order terms. Note that we do not assume that high-order terms are uniformly high-order [34], or negligible [36].

Finally, relying on well-establish control techniques [36], we achieve G2 by solving the trajectory tracking problem, i.e., G3. Based on the dynamic analysis, we prove the tracking error boundedness for the system class under analysis and a standard control algorithm.

A. Preliminary to Control Design for Complaint Robots

Recalling Assumption 1, (7), and (8), we start noting that one can write the following inequalities iteratively:

$$|\phi_k(x)| \leq \phi_{k_0}\|x\|, \quad \phi_{k_0} \triangleq f_0^k h_0 \tag{18}$$
$$|\psi_i(x)| \leq \psi_{i_0}\|x\|, \quad \psi_{i_0} \triangleq (i-r+1)f_0^{i-1}h_0 g_0. \tag{19}$$

$\forall x \in \mathscr{D}_x$, for $k = 0, \ldots, r'$, and $i = r, \ldots, r'$.

Lemma 1: Let us consider the system (1), (2), (6), and (6), under Assumptions 1, 2, and 4, then $\forall x \in \mathscr{D}_x$, it holds that

$$|\phi_k(x)| > \left|\phi_j(x)\right| \quad \forall k > j \quad k = 0, \ldots, r'. \tag{20}$$

Moreover, it holds that

$$\left|\frac{\phi_{k-1}(x)}{\phi_k(x)}\right| \leq \frac{1}{f_0} < 1, \quad k = 1, \ldots, r'. \tag{21}$$

Proof: Let us employ the induction principle on the differentiation order of (6), and let s be the inductive index.

$s = 0$ leads to $\phi_0(x) = h(x)$. Recalling Assumption 1, one has $|h(x)| \leq ||\nabla_x h(x)||||x|| \triangleq ||\nabla_x \phi_0(x)||||x|| \leq h_0||x||$.

$s = 1$ leads to $\phi_1(x) = L_f h(x)$. Recalling Assumption 1, one has $\phi_1(x) = \nabla_x h(x) f(x)$ and $|\phi_1(x)| \leq h_0 f_0||x|| = |\phi_0(x)|f_0$, which implies $(|\phi_0(x)|/|\phi_1(x)|) \leq (1/f_0) < 1$.

Let the inductive hypothesis be true.

$s = r'$ leads to $\phi_{r'}(x) = L_f^{r'} h(x)$. Recalling (6), one has $|\phi_{r'}(x)| = ||\nabla_x \phi_{r'-1}(x)||\|f(x)\| \leq |\phi_{r'-1_0}|f_0||x||$. ∎

Lemma 2: Let us consider the same Assumptions of Lemma 1, then it holds that

$$|\psi_i(x)| > |\psi_m(x)| \quad \forall i > m \quad i = r, \ldots, r'. \tag{22}$$

Moreover, it holds that

$$\left|\frac{\psi_{i-1}(x)}{\psi_i(x)}\right| \leq \frac{1}{f_0}\left(\frac{i-r}{i-r+1}\right) < 1 \quad i = r+1, \ldots, r'. \tag{23}$$

Proof: With analogous arguments of Lemma 1, recalling (20), (8), and Assumptions 1, we derive (22). Finally, recalling (19), (23) directly follows. ∎

Recalling (6), let us analyze $\theta_j(\cdot)$, for $j = r+1, \ldots, r'$.

Lemma 3: Let us consider the system (6) under Assumptions 1, 2, and 4. The terms $\theta_j(x, u^2, \ldots, u^{j-r+1}) : \mathscr{D}_x \times \mathbb{R} \times \cdots \times \mathbb{R} \to \mathbb{R}$ for $j = r+1, \ldots, r'$ are such that

$$\left|\theta_j\left(x, u^2, \ldots, u^{j-r+1}\right)\right| \leq \theta_{j_0}\left(u^2, \ldots, u^{j-r+1}\right)\|x\| \tag{24}$$

with the Lipschitz-like constant equal to

$$\theta_{j_0}\left(u^2, \ldots, u^{j-r+1}\right) \triangleq \sum_{i=1}^{j-r-1}(j-r)f_0^{j-i-1}h_0 g_0^{i+1}|u|^{i+1} + f_0^{r-1}h_0 g_0^{j-r+1}|u|^{j-r+1}. \tag{25}$$

Proof: Recalling (18) and (19), it holds that

$$\theta_{r+1_0}(\cdot) \leq f_0^{r-1}h_0 g_0^2|u|^2$$
$$\theta_{r+2_0}(\cdot) \leq 2f_0^{r-1}h_0 g_0^2|u|^2 + f_0^{r-1}h_0 g_0^3|u|^3 \tag{26}$$

which leads directly to (25). ∎

Lemma 4: Under the same Assumptions of Lemma 3, the terms $\theta_j(x, u^2, \ldots, u^{j-r+1})$ for $j = r+1, \ldots, r'$ can be written such as

$$\theta_j\left(x, u^2, \ldots, u^{j-r+1}\right) = \sum_{i=r+1}^{j} {}^j\alpha_{i-r+1}(x)u^{i-r+1} \tag{27}$$

where ${}^j\alpha_{i-r+1}(\cdot) : \mathscr{D}_x \to \mathbb{R}$ for $j = r+1, \ldots, r'$ is

$${}^j\alpha_{i-r+1}(x) = \sum_{k=1}^{{}^jb_{i-r+1}} {}_{i-r+1}^{j}\beta_k(x) \tag{28}$$

where ${}_{i-r+1}^{j}\beta_k(\cdot) : \mathscr{D}_x \to \mathbb{R}$ is locally Lipschitz and ${}^jb_{i-r+1} \in \mathbb{N}$ indicates the number of elements of each ${}^j\alpha_{i-r+1}(\cdot) \ \forall i, j$.

Moreover, it holds that

$$\left|\frac{{}_{i-r+1}^{j}\beta_k(x)}{\psi_j(x)}\right| \leq \left(\frac{j-r}{j-r+1}\right)\frac{g_0^i}{f_0^i} < 1. \tag{29}$$

$\forall j = r, \ldots, r' \ \forall i = r+1, \ldots, j \ \forall k = 2, \ldots, j \ \forall x \in \mathscr{D}_x$.

Proof: We proceed by induction on the output differentiation. Let s indicates the inductive step.

$s = r+1$ leads to $\theta_{r+1}(x, u^2) = L_g^2 L_f^{r-1}h(x)u^2 = {}^{r+1}\alpha_2(x)u^2$ with ${}^{r+1}_2\beta_1(x) = {}^{r+1}\alpha_2(x)$.

Let the inductive hypothesis be true.

$s = r'$ leads to (9) with $j = r'$. The term $\theta_{r'}(\cdot)$ is composed of two elements: the first is $\nabla_x \psi_{r'-1}(x)$, which has no dependence on the controller by construction, and the second is $\theta_{r'-1}(x, u^2, \ldots, u^{r'-r})$, which can be written, such as (27) and (28), thanks to the inductive hypothesis.

Finally, (29) comes directly recalling (19) and (25). The proof is completed. ∎

Remark 2: Analogous results of Lemma 1 also can be derived for the terms $\theta_j(\cdot)$ with $j = r+1, \ldots, r'$, formally $|\theta_{r'}(x, \cdot)| > \cdots > |\theta_r(x, \cdot)| \ \forall x \in \mathscr{D}_x$. This can be proved via (9) and using the same inductive approach of Lemma 1–3.

B. Control Design: Inverse Dynamic Controller

The following Theorem presents the classic input-state feedback controller [36] coping with the evolution of high-order terms in (6).

Theorem 1: Let us consider the system (2) and (3), with normal form (6)–(11), under Assumptions 1–4. Let the feedback controller be [36]

$$u(z,\xi_d)=\frac{v^{(r')}(\xi,\xi_d)-\phi_{r'}(z)}{\psi_{r'}(z)} \tag{30}$$

where $v^{(r')}\in\mathbb{R}$ is an additional control input equal to

$$v^{(r')}=\xi_d^{(r')}+\Upsilon e^{(r')}\,,\quad e^{(r')}=\left[e_0,,\ldots,e_{r'-1}\right]^\top\in\mathbb{R}^{1\times r'} \tag{31}$$

with the error $e^{(r')}\in\mathbb{R}^{r'}$, such as $e_m^{(r')}\triangleq\xi_d^{(m)}-\xi^{(m)}$ for $m=0,\ldots,r'-1$, and the control gain $\Upsilon\in\mathbb{R}^{1\times r'}$ and $\Upsilon\succ 0$.

Then, the following inequalities hold:

$$\begin{aligned}\|\Psi(z)u\|_{u(z)}&\le\overline{\psi}\left|v^{(r')}-\phi_{r'}(z)\right|,\ \overline{\psi}\\&\triangleq\left(\frac{r'-r}{r'-r+1}\right)\frac{1}{f_0}<1\end{aligned} \tag{32}$$

$$\|\Theta(z,\cdot)\|_{u(z)}\le\overline{\theta}\sum_{i=1}^{r'-r}\left|v^{(r')}-\phi_{r'}(z)\right|^{i+1}$$

$$\overline{\theta}\triangleq\frac{(r'-r)(r'-r-1)}{(r'-r+1)^2}\frac{1}{f_0^{r'}h_0}<1. \tag{33}$$

Proof: Recalling (11), substituting it in (30), by means of Lemma 3, one has

$$\dot{\xi}_l=\begin{cases}\xi_{l+1}\quad\text{if } l=1,\ldots,r-1\\ \xi_{l+1}+\psi_l(z)\left(\frac{v^{(r')}-\phi_{r'}(z)}{\psi_{r'}(z)}\right)\quad\text{if } l=r\\ \xi_{l+1}+\psi_l(z)\left(\frac{v^{(r')}-\phi_{r'}(z)}{\psi_{r'}(z)}\right)\\ \quad+\sum_{i=r+1}^{l}\sum_{k=1}^{l_{b_l}}{}_{i-r+1}^{l}\beta_k(z)\\ \quad\times\left(\frac{v^{(r')}-\phi_{r'}(z)}{\psi_{r'}(z)}\right)^{i-r+1}\quad\text{if } l=r+1,\ldots,r'-1\\ -\Upsilon\xi\\ \quad+\sum_{i=r+1}^{l}\sum_{k=1}^{l_{b_l}}{}_{i-r+1}^{l}\beta_k(z)\\ \quad\times\left(\frac{v^{(r')}-\phi_{r'}(z)}{\psi_{r'}(z)}\right)^{i-r+1}\quad\text{if } l=r'.\end{cases} \tag{34}$$

Starting from (34), and Lemmas 1–3, one can write the following inequalities for $l=r\ldots r'-1$:

$$\frac{|\psi_l(z)|}{|\psi_{r'}(z)|}\le\left(\frac{l-r+1}{r'-r+1}\right)\left|\frac{1}{f_0^{r'-l}}\right| \tag{35}$$

$$\begin{aligned}|\theta_l(z,\cdot)|_u\le&\sum_{i=1}^{l-r-1}\frac{(l-r)f_0^{l-i-1}h_0g_0^{i+1}}{\left((r'-r+1)f_0^{r'-1}h_0g_0\right)^{i+1}}\left|v^{(r')}-\phi_{r'}(z)\right|^{i+1}\\&+\frac{f_0^{r-1}h_0g_0^{l-r+1}}{\left((r'-r+1)f_0^{r'-1}h_0g_0\right)^{l-r+1}}\left|v^{(r')}-\phi_{r'}(z)\right|^{l-r+1}.\end{aligned} \tag{36}$$

Thanks to th results of Lemma 3 and 4, we know that the largest coefficient among the ones in the summation in (36) appears for $i=1$. Therefore, recalling (36), one can derive the following inequality with $l=r+1,\ldots,r'$:

$$\begin{aligned}|\theta_l(z,\cdot)|\le&\frac{(l-r-1)(l-r)f_0^{l-2}g_0^2h_0}{\left((r'-r+1)h_0g_0f_0^{r'-1}\right)^2}\sum_{i=1}^{l-r-1}\left|v^{(r')}-\phi_{r'}(z)\right|^{i+1}\\&+\frac{f_0^{r-1}h_0g_0^{l-r+1}}{\left((r'-r+1)f_0^{r'-1}h_0g_0\right)^{l-r+1}}\left|v^{(r')}-\phi_{r'}(z)\right|^{l-r+1}.\end{aligned} \tag{37}$$

Finally, considering (34), (36), and (37) one has

$$\begin{aligned}\left|\left|\dot{\xi}\right|\right|&\le||\Upsilon||||\xi||+\overline{\psi}\left|v^{(r')}-\phi_{r'}(z)\right|\\&\quad+\frac{(r'-r)(r'-r-1)}{(r'-r+1)^2}\frac{1}{f_0^{r'}h_0}\sum_{i=1}^{r'-r}\left|v^{(r')}-\phi_{r'}(z)\right|^{i+1}\\&=||\Upsilon||||\xi||+\overline{\psi}\left|v^{(r')}-\phi_{r'}(z)\right|+\overline{\theta}\sum_{i=1}^{r'-r}\left|v^{(r')}-\phi_{r'}(z)\right|^{i+1}\end{aligned} \tag{38}$$

where $\overline{\psi},\overline{\theta}\in(0,1)$ is, such as in (32) and (33). ■

Theorem 1 achieves G2.

Let us consider the trajectory tracking problem employing the classic controller (30) and the error (31). To achieve G3, we introduce the following theorem.

Theorem 2: Let us consider the system (2) and (3), with normal form (6) and (11), under Assumptions 1–4. Let (30) be the feedback controller. Let $A_{cl}\in\mathbb{R}^{r'\times r'}$ be the closed-loop matrix when applying (30) to (11). Let $P,Q\in\mathbb{R}^{r'\times r'}$ be symmetric such that $P,Q\succ 0$, and $PA_{cl}+A_{cl}^\top P=-Q$. Let us suppose that $\text{eig}\{\partial p(\cdot,\eta)/\partial\eta\}$ are stable.

If the following inequality holds true:

$$\overline{\psi}\left|\overline{\upsilon}-f_0^{r'}h_0\right|+\overline{\theta}\sum_{i=1}^{r'-r}\left|\overline{\upsilon}-f_0^{r'}h_0\right|^{i+1}\le\|Q\|/(2\|P\|) \tag{39}$$

then the controller (30) solves the trajectory tracking problem for the system (2) and (3) with a bounded error $O(e^{(r')})$.

Proof: Let us consider the closed-loop system

$$\begin{aligned}\dot{e}^{(r')}=&A_{\text{cl}}e^{(r')}+\Psi\left(e^{(r')},\eta\right)\left(\frac{v^{(r')}-\phi_{r'}\left(e^{(r')},\eta\right)}{\psi_{r'}\left(e^{(r')},\eta\right)}\right)\\&+\Theta\left(e^{(r')},\eta,u^2,\ldots,u^{r'-r+1}\right)\Big|_{u=\frac{v^{(r')}-\phi_{r'}\left(e^{(r')},\eta\right)}{\psi_{r'}\left(e^{(r')},\eta\right)}}\\\triangleq&A_{\text{cl}}e^{(r')}+\Psi_{\text{cl}}\left(e^{(r')},\eta\right)+\Theta_{\text{cl}}\left(e^{(r')},\eta\right)\end{aligned} \tag{40}$$

where A_{cl} is such that $A_{cl_{ij}}=1$ if $j=i+1$, $A_{cl_{ij}}=\upsilon_{j-1}$ if $i=n\wedge j=1,\ldots,2n$, and $A_{cl_{ij}}=0$ otherwise. Recalling Assumption 3, there exists a proper choice of υ_m for $m=0,\ldots,r'-1$, which makes the matrix A_{cl} Hurwitz. Note that $\Theta_{\text{cl}}(\cdot)$ depends on the power of the control input.

Let be $V(z)=V(e^{(r')},\eta)=V_{\text{e}}(e^{(r')})+V_\eta(\eta)$, such as $V_{\text{e}}(e^{(r')})=e^{(r')^\top}Pe^{(r')}$ a Lyapunov function, i.e., $V(\cdot):\mathbb{R}^{r'}\times\mathbb{R}^{2n-r'}\to\mathbb{R}$, $V(0_{2n-r'\times 1})=0$, and $V(e^{(r')},\eta)>0\ \ \forall z\neq$

$0_{2n-r'\times 1}$. Differentiating the Lyapunov candidate leads to $\dot{V}(e^{(r')},\eta)=\dot{V}_e(e^{(r')})+\dot{V}_\eta(\eta)$, with $\dot{V}_\eta(\eta)<0$, and $\dot{V}_e(e^{(r')})=2e^{(r')\top}P\dot{e}^{(r')}$, i.e.,

$$\begin{aligned}\dot{V}_e(e^{(r')}) &= 2e^{(r')\top}PA_{\rm cl}e^{(r')}\\ &\quad+2e^{(r')\top}P(\Psi_{cl}(e^{(r')},\eta)+\Theta_{cl}\left(e^{(r')},\eta\right))\\ &\le -||e^{(r')}||^2\|Q\|\\ &\quad+2||e^{(r')}||\|P\|\left(||\Psi_{cl}\left(e^{(r')},\eta\right)||+||\Theta_{cl}\left(e^{(r')},\eta\right)||\right).\end{aligned}\tag{41}$$

To complete the proof, one has to show that $\dot{V}\le 0$, i.e.,

$$\begin{aligned}&||Q||\left|\left|e^{(r')}\right|\right|/(2||P||)\\ &\ge \overline{\psi}\left|v^{(r')}-\phi_{r'}\left(e^{(r')},\eta\right)\right|+\overline{\theta}\sum_{i=1}^{r'-r}\left|v^{(r')}-\phi_{r'}\left(e^{(r')},\eta\right)\right|^{i+1}\end{aligned}\tag{42}$$

therefore, recalling the inverse triangular inequality[2] on the right side of (42), the following holds:

$$\begin{aligned}&\left(\overline{\psi}\left|\overline{v}-\phi_{r'_0}\right|+\overline{\theta}\sum_{i=1}^{r'-r}\left|\overline{v}-\phi_{r'_0}\right|^{i+1}\right)\left(||e^{(r')}||+||\eta||\right)\\ &\le\frac{||Q||\left(||e^{(r')}||+||\eta||\right)}{2||P||}\end{aligned}\tag{43}$$

which leads directly to (39) via (18). Relying on the LaSalle invariant principle, one can guarantee the asymptotic trajectory with an $O(e^{(r')})$ error devoted to the neglected terms $\omega_j(\cdot)$ with $j=r+1,\dots,r'$ in Assumption 4. ■

Remark 3: Recalling (30) with $r'=r$, then (30) is the classic input–output feedback linearization controller see [48].

Remark 4: Recalling (30) with $r'=2n$, then (30) is similar to the approach proposed in [36] or [35], but with different $\psi_{r'}(z)$. However, in this work, we exploit the mechanical properties of the compliant arms, and we do not require any strong assumptions on both $\psi_i(x)$ for $i=r,\dots,2n$, and $\theta_j(\cdot)$ with $j=r+1,\dots,2n$.

Remark 5: Recalling (30), if it relies on a switching policy w.r.t. the relative degree, i.e., (6), then the controller is similar to the one proposed in [34]. Therefore analogous results of Theorem 2 could be derived requiring the slow switching hypothesis w.r.t. relative degree, [34]. The main differences between this work and [34] are the ones listed in Remark 4

Remark 6: The controller (30) requires knowledge of the model and real-time output derivatives. However, thanks to Proposition 1 and 2, the number of the order of the derivative can be selected to be 4. In addition, the model itself could be used to derive the high-order derivatives.

V. Validation

In this section, we test the analysis effectiveness in both simulations and real hardware.

Simulations and experimental tests are performed on two and three DoFs arms, namely $R\overline{R}$ [56], $R\overline{R}\overline{R}$ [3], and $3PCC$, in which only the first elastic joint is active while the others are unactuated. Note that the two systems, namely $R\overline{R}$ and $R\overline{R}\overline{R}$, are modeled with an LP model and they are articulated robots with one or two unactuated join. Conversely, the third robot is a continuum one, which is still an underactuated system and composed of 3 *PCC* segments model [4]. For the $R\overline{R}$ and $R\overline{R}\overline{R}$, the dynamic parameters for each link are $m_i=0.55\,\text{kg}$, $J_i=0.01\,\text{kg m}^2$, $l_i=0.089\,\text{m}$, $a_i=0.085\,\text{m}$, $k_{ii}=1\,\text{Nm/rad}$, and $d_{ii}=0.1\,\text{Nms/rad}$ are the mass, inertia, length, center of mass distance, spring, and damper of each link, respectively for $i=1,2,3$; note that $S=[1,\,0]^\top$ and $S=[1,\,0,\,0]^\top$ for $R\overline{R}$ and $R\overline{R}\overline{R}$, respectively. Assumption 3 holds for all the compliant arms selected by direct computation.

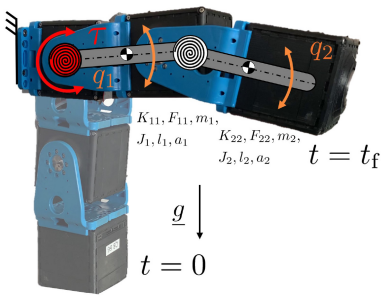

Fig. 2. Experimental setup, namely $R\overline{R}$. The robot is composed of one elastic active joint (red circle) and one passive elastic joint (white circle).

For the $3PCC$, we have three PCC segments, where $m_1=0.25$, $m_i=0.15\,\text{kg}$, $l_1=0.25$, $l_i=0.15\,\text{m}$, $J_i=1(1/12)m_i l_i^2\,\text{kg m}^2$, $k_{ii}=1\,(\text{Nm/rad})$, and $d_{ii}=0.1\,(\text{Nms/rad})$ with $i=1,2,3$ and the usual meaning; note that $S=[1,\,0,\,0]^\top$.

The output function (6) is the robot tip orientation, i.e.,

$$y=\left[1_{1\times n}\;0_{1\times n}\right]x\,,\quad y\in\mathbb{R}.\tag{44}$$

We employ three different reference trajectories.

1) A constant trajectory solving the classic swing-up task, i.e., from $y_0\triangleq y(0)=0\text{rad}$ to $y_f\triangleq y(t_f)=\pi\,\text{rad}$ in $t_f=10\text{s}$.
2) A constant trajectory from $y_0=0\text{rad}$ to $y_f=1\text{rad}$ ($\approx 60°$) with $t_f=5\text{s}$.
3) A constant trajectory from $y_0=-\pi/6\text{rad}$ to $y_f=\pi/3\text{rad}$ with $t_f=5\text{s}$.
4) A minimum crackle starting from $y_0=0\text{rad}$ and reaching $y_f=(\pi/2)\text{rad}$ in $t_f=1\text{s}$, i.e., [57].

Note that Section III tackles the trajectory tracking problem. However, the regulation task is a special case of tracking one.

We employ the control law (30) with gains $\Upsilon\in\mathbb{R}^{1\times r'}$, which are chosen depending on the task and summarized by Table I.

Finally, it is worth noting that the method's effectiveness is validated by varying tasks, systems, number of passive joints, relative degrees, and stiffness profiles. We also compared the results with classic state-of-the-art controllers for underactuated robots, i.e., proportional derivative [58] and AFL [35].

[2] $\forall a,b\in\mathbb{C}^n$, it holds $|a-b|\ge|\|a\|-\|b\||$.

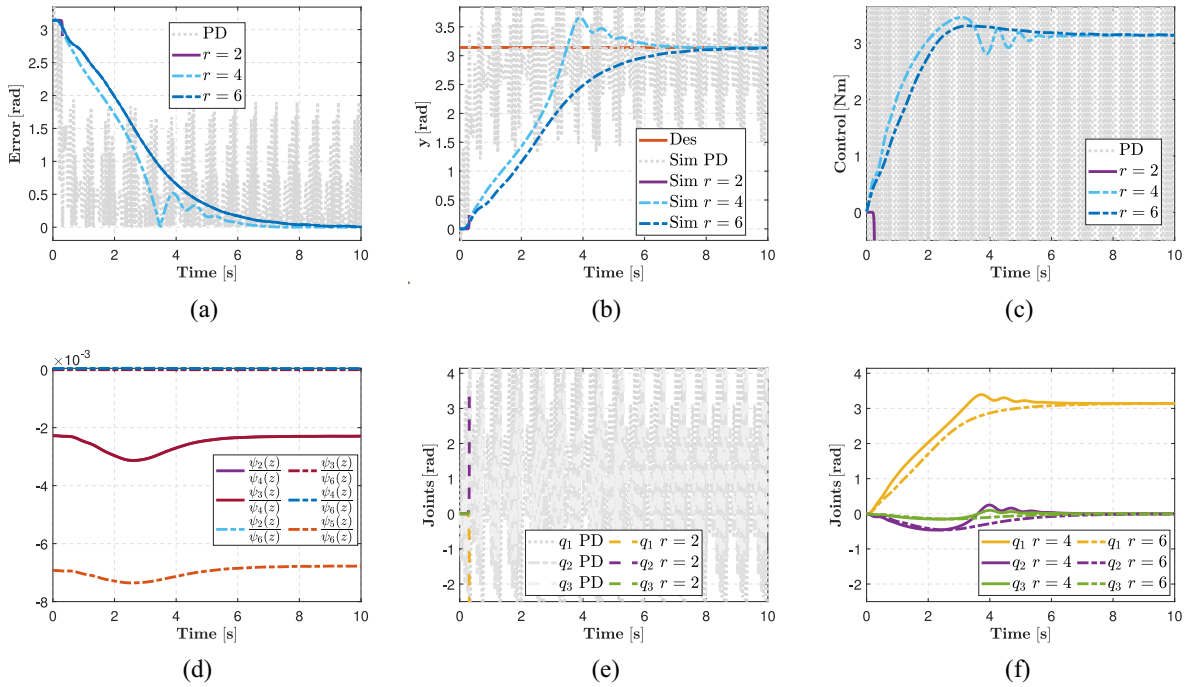

Fig. 3. $R\overline{RR}$ simulation results for the swing up task. We test different robust relative degrees and compare the results with the PD controller. (a) Error evolution over time. (b) Output tracking performance. (c) Control action. (d) $[\psi_2(x)/\psi_4(x)]$, $[\psi_3(x)/\psi_4(x)]$, and $[\psi_j(x)/\psi_6(x)]$ for $j = 2, \ldots, 5$. (e) Joints evolution over time. (f) Joints evolution over time.

TABLE I
CONTROL GAINS

Robot	Type	υ_0	υ_1	υ_2	υ_3	υ_4	υ_5
$R\overline{R}$	Sim	1e6	2e5	2e4	1	-	-
$R\overline{RR}$	Sim	8e7	1e8	2e6	2e5	2e4	1
$R\overline{R}$ Reg	Exp	1e10	2e8	2e7	1e3	-	-
$R\overline{R}$ Track	Exp	7e7	7e6	7e4	1e4	-	-
3*PCC* Reg	Sim	5e4	1e3	1	-	-	-

A. Simulation Results $R\overline{RR}$

In this section, the capability of the controller (30) to deal with more than one passive joint is tested. To this end, the dynamics of a three DoFs robot with only the first elastic joint active is simulated with unstable vertical equilibrium [19]. Recalling (6), the robust relative degree is $r' = 4, 6$, the output function is (44), and the task is the swing-up, i.e., 1).

We also compare the results with a classic proportional-derivative (PD) controller, i.e., $u = K_{\mathrm{P}}(y_{\mathrm{d}} - y) + K_{\mathrm{V}}(\dot{y}_{\mathrm{d}} - \dot{y})$ with $K_{\mathrm{P}} = 1$ and $K_{\mathrm{V}} = 0.5$[3].

Fig. 3 shows the simulation results. Fig. 3(a) depicts the error's time evolution, Fig. 3(b) reports the output, Fig. 3(c) shows the control action, Fig. 3(d) shows the high-order terms time evolution, and Fig. 3(e) and (f) depicts the joints evolution. Finally, Fig. 6(a) shows a photograph-sequence of the swing-up task with $r' = 6$, i.e., a complete change of variables (6).

Simulation 3*PCC*

In this section, the capability of the controller (30) to deal with a continuum robot and more than one passive joint is tested. Recalling (6), the robust relative degree is selected, such as $r' = 3$ the output function is (44), and we perform a regulation task, i.e., 3). We also compare the computed torque case, i.e., $r' = r = 2$.

Applying (6) and recalling Definitions 2 and 3, it holds that $\psi_2(x) = q_1 {}^{3\mathrm{PCC}}\psi_2(x)$ and $\psi_3(x) = (q_1 + \dot{q}_1) {}^{3\mathrm{PCC}}\phi_3(x)$ where ${}^{3\mathrm{PCC}}\psi_2(x)$, ${}^{3\mathrm{PCC}}\psi_3(x)$ collect the rest of the expression. Thus, one has that if $q_1 \to 0$ then, $\psi_2(x) \to +\infty$, i.e., crossing the vertical equilibrium; conversely, if it holds that $\dot{q}_1 \neq 0$, the controller (30) is well defined in crossing the vertical equilibrium.

Fig. 4 reports the output, Fig. 4(a) shows the output regulation performances, and Fig. 4(b) depicts the joints' evolution. Finally, Fig. 4(c) shows a 3-D visualization for 3*PCC* in the case of $r' = 3$.

B. Experiment Results $R\overline{R}$

We here compare the simulations and experimental results for the $R\overline{R}$ system depicted in Fig. 1.

Fig. 1 shows the experimental setup, which utilizes qb-Move Advanced [59] actuators. This is a variable stiffness actuator with elastic torque $\tau_e = 2\iota_1 \cosh(\kappa\delta_{\mathrm{s}}) \sinh(\kappa(q - \delta_{\mathrm{e}}))$ and nonlinear stiffness profile $\sigma = 2\kappa\iota_1 \cosh(\kappa\delta_{\mathrm{s}}) \cosh(\kappa(q - \delta_{\mathrm{e}}))$, where $\kappa = 6.7328$ 1/rad, and $\iota_1 = 0.0222$ Nm. Note that δ_{s} tunes the desired stiffness, and, to approximate a serial elastic actuator in (1), it is set constant. The second link is punctuated, i.e., a qbMove Advanced actuator with δ_{s} constant and δ_e null. Thus, we have a passive joint with a torsional spring and a position encoder sensor. Note that in (1), the stiffness is assumed to be linear, while the real one is not. Therefore, the actuator model is not exact and introduces an error in the controller (30).

[3]The gains are selected in such a way to avoid numerical singularity.

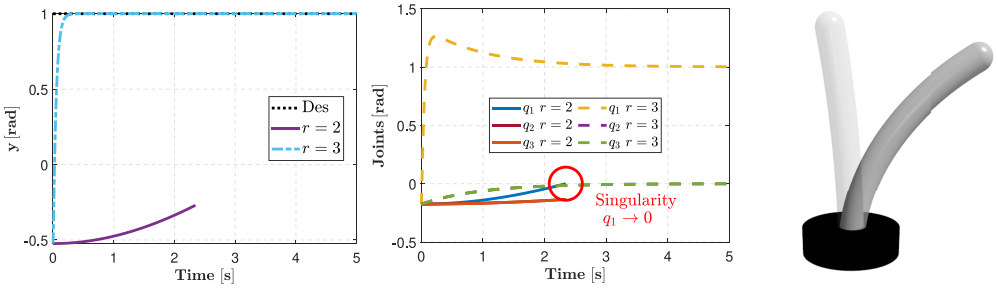

(a) (b) (c)

Fig. 4. $3PCC$ simulation results for the regulation task. We test different robust relative degrees, i.e., $r' = 2$, $r' = 3$. The case $r' = 2$ leads to the classic AFL controllers. In Fig. 4(c), the transparent robot displays the arm in its initial condition. (a) Output tracking. (b) Joints evolution over time. (c) 3-D visualization.

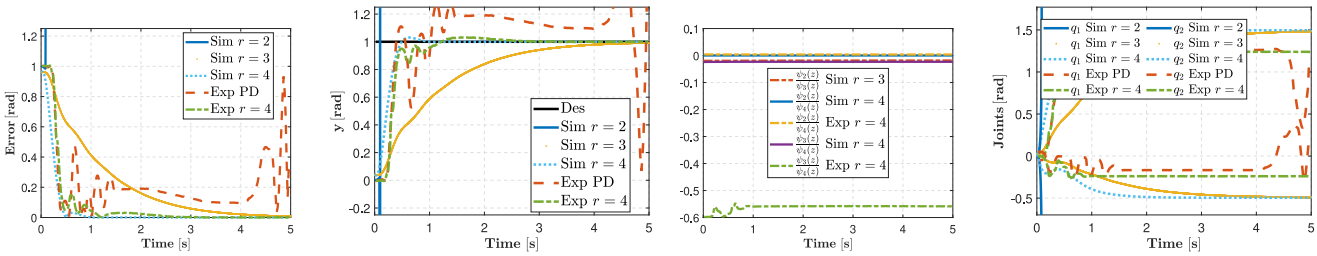

(a) (b) (c) (d)

Fig. 5. $R\overline{R}$ simulation and experimental results for the regulation task. We test different robust relative degrees and compare the result with a PD control. (a) Error evolution over time. (b) Output tracking performance. (c) $[\psi_2(x)/\psi_3(x)]$ and $[\psi_j(x)/\psi_4(x)]j = 2, 3$. (d) Joints evolution over time.

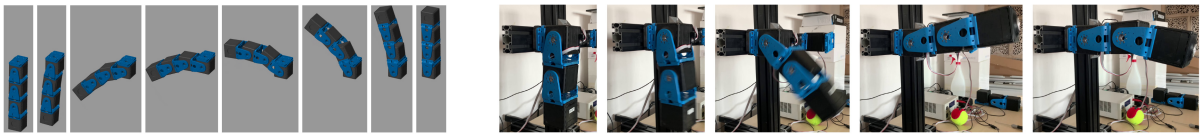

(a) (b)

Fig. 6. Photograph sequence showing the execution of the swing-up task $R\overline{R}\overline{R}$ sim Fig. 6(a) and regulation $R\overline{R}$ experiment Fig. 6(b). (a) Sim. $R\overline{R}\overline{R}$ swing-up. (b) Exp. $R\overline{R}$ regulation.

In the simulations, the value of the robust relative degree is $r' = 3, 4$. At the same time, in the experiment, it is $r' = 4$, i.e., full state approximation (6), the output function is (44), and both the desired trajectories are performed, namely regulation with $t_f = 5$ s, i.e., 2, and trajectory tracking, i.e., 4. In the former $\delta_s = 25°$, in the latter, $\delta_s = 20°$. This leads to $k_{ii} = 2.7$ Nm/rad and $k_{ii} = 1.5$ Nm/rad, with $i = 1, 2$, respectively.

1) Regulation Results: This task is compared with a PD controller, i.e., $u = K_P(y_{des} - y) + K_V(\dot{y}_{des} - \dot{y})$ with $K_P = 5$ and $K_V = 0.5$.

Fig. 5 compares the results of the simulation and the experiment for the trajectory 2). Fig. 5(a) depicts the error evolution, Fig. 5(b) reports the output, Fig. 5(c) shows the time evolution of the high-order terms in (6), and Fig. 5(d) depicts the joints evolution. Finally, Fig. 6(b) shows a photograph-sequence of the regulation task execution.

2) Trajectory Tracking Results: This task is compared with an approximating computed torque controller, i.e., fixing $r = r' = 2$. In particular, $\psi_2(x) = [b_2 \cos(q_2)/\text{detM}]$, where b_2, detM $\in \mathbb{R}$, [56]. We implement an AFL controller modified the $g(x)$ field [58], i.e., $\psi_2(x) \approx (b_2/\text{detM})$. Note that this leads to no singularities.

Fig. 7 compares the results of the simulation and the experiment for the trajectory 4. Fig. 7(a) depicts the error evolution, Fig. 7(b) reports the output, Fig. 7(c) shows the time evolution of the high-order terms, and Fig. 7(d) depicts the joints evolution.

C. Discussion

Results show that the controller can reach the desired position Figs. 3–5 and track the desired trajectory Fig. 7. Results show good performances while executing fast and challenging tasks, with satisfying values of the tracking error Figs. 3(a), 5(a), and 7(a).

The feedback controller (30) can compensate for the passive elements in the arm rejecting oscillation and achieving the goal. It is worth noting that leveraging high-order dynamics terms in the control action (30) leads to an always well-defined relative degree during the whole task. Conversely, in the case of $r = 2$, the controller encounters singularity during the task execution (Fig. 5).

We highlight that the value of f_0 is such that $f_0 \approx 3$. Then, choosing $Q = I_{r'}$, and $\overline{v}$, depending on the task (Table I), lead to fulfill the inequality (39).

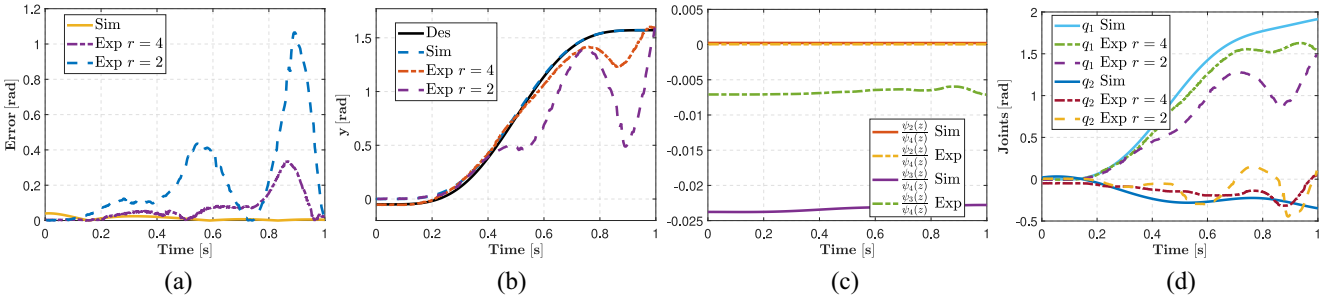

Fig. 7. $R\overline{R}$ simulation and experimental results for the trajectory tracking task. We test different robust relative degrees, we compare the results with $r = r' = 2$, i.e., computed torque controller. (a) Error evolution over time. (b) Output tracking performance. (c) $[\psi_j(x)/\psi_4(x)]$ for $j = 2, 3$. (d) Joints evolution over time.

The controller (30) deeply relies on both the model accurateness and the precise estimation of the output derivatives. Therefore, the convergence of the error is smoother in simulations where both the knowledge of the model and the numerical estimation of the derivatives are accurate. However, satisfying tracking performances are achieved also in the experimental cases and very challenging scenarios, e.g., Fig. 7. Furthermore, the diffeomorphism is well defined throughout all tasks.

The derivation of the coupling condition is purely model-based as well as the controller (30). Thus, it is sensitive to error modeling and is time-consuming when increasing the number of robot's DoFs. However, relying on Propositions 1 and 2, one can reshape the stiffness profile to fix the robust relative degree. This is demonstrated with the $R\overline{R}\overline{R}$ robot Fig. 3.

Propositions 1 and 2 are verified thanks to the fact that the swing-up task is achieved with $r' = 4$, 6 in Fig. 3; as well as the regulation one for $r' = 3$, 4 in Fig.5. In addition, Figs. 3 and 5 show how the case $r = 2$ encounters singularities. Note that the choice $r = 4$, 6 can also be a user's design choice of the controller.

The applicability of the conditions from Definitions 1 to 4 is twofold. One is to derive well-defined control actions in a model-based paradigm. The second is to study the singularity of a compliant underactuated robot and, thus, create strategies to avoid them. In other words, the condition can be employed as a debugging tool, which may be embedded into an optimal framework [60]. Moreover, Propositions 1 and 2 can serve to ensure a correct synthesis of the conditions from Definitions 1 to 4 as well as of the diffeomorphism (11). The coupling conditions enable the possibility to control multiple typologies of robots, i.e., lightweight with unactuated joints and continuum ones, which we call compliant underactuated robots. It is worth noting that the control action in Fig. 4 is very demanding, but it can compensate for the singularity in the control action.

The PD controller in Fig. 5 does not need any description of the model in most practical cases, however, it performs poorly. It is worth noting that the model-free nature of such a PD controller may not fulfill the coupling conditions from Definitions 1 to 4. Moreover, the AFL with $r = 2$ leads to lacking dynamics description in the controller which reduces performance. For the $R\overline{R}\overline{R}$, the PD controller does not solve the swing-up task, Fig. 3. This implies that considering only the inertial term in the control action does not manage the relative degree leading to singularities of the controller. In other words, the inertial-based controller is too aggressive and creates a strong motion displacing the passive joints and leading to control singularities. PD and AFL are state-of-the-art controllers for controlling underactuated systems [29], [35], [36], [58].

Finally, the high-order terms in (6), i.e., $\psi_i(x)$ for $i = r, \ldots, r'$ and $\theta_j(\cdot)$ for $j = r+1, \ldots, r'$, are small as depicted in Figs. 3(d), 5(c), and 7(c). Thus, Assumption 4 and the thesis of Theorem 2 are verified leading to good tracking results. Note that the terms $\theta_j(\cdot)$ for $j = r+1, \ldots, r'$ are not reported in the Figs. 3, 5, and 7 since $|\psi_i(x)| > |\theta_j(\cdot)| \quad \forall i = r, \ldots, r'$ and $\forall j = r+1, \ldots, r'$, i.e., Lemmas 1–3. Finally, the error is comparable with the value of the high-order terms Figs. 3(d), 5(c), and 7(c).

VI. Conclusion

In this work, we proposed new controllability-like conditions for a class of compliant underactuated arms coping with a not well-defined relative degree. We generalize the well-known strong inertial coupling condition guaranteeing a piecewise-constant relative degree greater than two. We investigate the role of the stiffness and damping matrices in the change of relative degree. Then, we use a classic input–output feedback linearization controller to solve the trajectory tracking problem relying on the new dynamic conditions proving its closed-loop stability. Finally, the effectiveness of the approach is tested both in simulation and on real hardware using varying underactuated compliant arms, stiffness profiles, and tasks. Future research will focus on designing a switching policy due to the relative degree of dependency and machine learning approximation [20] to estimate the $\phi_k(\cdot)$, $k = r, \ldots, r'$ terms considering the actuator dynamics and 3-D robot's motions.

References

[1] D. Rus and M. T. Tolley, "Design, fabrication and control of soft robots," *Nature*, vol. 521, no. 7553, pp. 467–475, 2015.
[2] C. D. Santina, *Flexible Manipulator*, vol. 20. Berlin, Germany: Springer, 2021.
[3] M. Pierallini, F. Angelini, R. Mengacci, A. Palleschi, A. Bicchi, and M. Garabini, "Iterative learning control for compliant underactuated arms," *IEEE Trans. Syst., Man, Cybern., Syst.*, vol. 53, no. 6, pp. 3810–3822, Jun. 2023.
[4] M. Pierallini et al., "A provably stable iterative learning controller for continuum soft robots," *IEEE Robot. Autom. Lett.*, vol. 8, no. 10, pp. 6427–6434, Oct. 2023.

[5] F. Angelini, C. Petrocelli, M. G. Catalano, M. Garabini, G. Grioli, and A. Bicchi, "SoftHandler: An integrated soft robotic system for handling heterogeneous objects," *IEEE Robot. Autom. Mag.*, vol. 27, no. 3, pp. 55–72, Sep. 2020.

[6] B. Zhang, Y. Fan, P. Yang, T. Cao, and H. Liao, "Worm-like soft robot for complicated tubular environments," *Soft Robot.*, vol. 6, no. 3, pp. 399–413, 2019.

[7] J. P. Vasconez, G. A. Kantor, and F. A. Auat Cheein, "Human–robot interaction in agriculture: A survey and current challenges," *Biosyst. Eng.*, vol. 179, pp. 35–48, Mar. 2019.

[8] Z. Pang, G. Yang, R. Khedri, and Y.-T. Zhang, "Introduction to the special section: Convergence of automation technology, biomedical engineering, and health informatics toward the healthcare 4.0," *IEEE Rev. Biomed. Eng.*, vol. 11, pp. 249–259, 2018.

[9] S. Xu, C. M. Nunez, M. Souri, and R. J. Wood, "A compact DEA-based soft peristaltic pump for power and control of fluidic robots," *Sci. Robot.*, vol. 8, no. 79, 2023, Art. no. eadd4649.

[10] F. Stella and J. Hughes, "The science of soft robot design: A review of motivations, methods and enabling technologies," *Front. Robot. AI*, vol. 9, Jan. 2023, Art. no. 1059026.

[11] C. Armanini, F. Boyer, A. T. Mathew, C. Duriez, and F. Renda, "Soft robots modeling: A structured overview," *IEEE Trans. Robot.*, vol. 39, no. 3, pp. 1728–1748, Jun. 2023.

[12] S. M. H. Sadati, S. E. Naghibi, L. da Cruz, and C. Bergeles, "Reduced order modeling and model order reduction for continuum manipulators: An overview," *Front. Robot. AI*, vol. 10, Sep. 2023, Art. no. 1094114.

[13] L. Qin, H. Peng, X. Huang, M. Liu, and W. Huang, "Modeling and simulation of dynamics in soft robotics: A review of numerical approaches," *Current Robot. Rep.*, vol. 5, pp. 1–13, Mar. 2024.

[14] C. D. Santina, C. Duriez, and D. Rus, "Model-based control of soft robots: A survey of the state of the art and open challenges," *IEEE Control Syst. Mag.*, vol. 43, no. 3, pp. 30–65, Jun. 2023.

[15] C. D. Santina, R. K. Katzschmann, A. Bicchi, and D. Rus, "Model-based dynamic feedback control of a planar soft robot: Trajectory tracking and interaction with the environment," *Int. J. Robot. Res.*, vol. 39, no. 4, pp. 490–513, 2020.

[16] T. G. Thuruthel, E. Falotico, F. Renda, and C. Laschi, "Model-based reinforcement learning for closed-loop dynamic control of soft robotic manipulators," *IEEE Trans. Robot.*, vol. 35, no. 1, pp. 124–134, Feb. 2019.

[17] F. Han and J. Yi, "On the learned balance manifold of underactuated balance robots," in *Proc. IEEE Int. Conf. Robot. Autom. (ICRA)*, 2023, pp. 12254–12260.

[18] F. Angelini et al., "Decentralized trajectory tracking control for soft robots interacting with the environment," *IEEE Trans. Robot.*, vol. 34, no. 4, pp. 924–935, Aug. 2018.

[19] M. Pierallini, F. Angelini, A. Bicchi, and M. Garabini, "Swing-up of underactuated compliant arms via iterative learning control," *IEEE Robot. Autom. Lett.*, vol. 7, no. 2, pp. 3186–3193, Apr. 2022.

[20] J. Liu, P. Borja, and C. D. Santina, "Physics-informed neural networks to model and control robots: A theoretical and experimental investigation," *Adv. Intell. Syst.*, vol. 6, no. 5, 2024, Art. no. 2300385.

[21] S. Satheeshbabu, N. K. Uppalapati, G. Chowdhary, and G. Krishnan, "Open loop position control of soft continuum arm using deep reinforcement learning," in *Proc. Int. Conf. Robot. Autom. (ICRA)*, 2019, pp. 5133–5139.

[22] Y. Li, X. Wang, and K.-W. Kwok, "Towards adaptive continuous control of soft robotic manipulator using reinforcement learning," in *Proc. IEEE/RSJ Int. Conf. Intell. Robots Syst. (IROS)*, 2022, pp. 7074–7081.

[23] R. K. Katzschmann, C. D. Santina, Y. Toshimitsu, A. Bicchi, and D. Rus, "Dynamic motion control of multi-segment soft robots using piecewise constant curvature matched with an augmented rigid body model," in *Proc. 2nd IEEE Int. Conf. Soft Robot. (RoboSoft)*, 2019, pp. 454–461.

[24] G. Bastos Jr. and E. Franco, "Dynamic tube model predictive control for a class of soft manipulators with fluidic actuation," *Int. J. Robust Nonlinear Control*, 2023, to be published.

[25] E. Franco, A. Aktas, S. Treratanakulchai, A. Garriga-Casanovas, A. Donder, and F. R. y Baena, "Discrete-time model based control of soft manipulator with fbg sensing," in *Proc. IEEE Int. Conf. Robot. Autom. (ICRA)*, 2023, pp. 567–572.

[26] M. W. Spong, "Partial feedback linearization of underactuated mechanical systems," in *Proc. IEEE/RSJ Int. Conf. Intell. Robots Syst. (IROS)*, 1994, pp. 314–321.

[27] D. Gutiérrez-Oribio, J. A. Mercado-Uribe, J. A. Moreno, and L. Fridman, "Robust global stabilization of a class of underactuated mechanical systems of two degrees of freedom," *Int. J. Robust Nonlinear Control*, vol. 31, no. 9, pp. 3908–3928, 2021.

[28] J. A. Moreno, E. Cruz-Zavala, and Á. Mercado-Uribe, "Discontinuous integral control for systems with arbitrary relative degree," in *Variable-Structure Systems Sliding-Mode Control: From Theory to Practice*. Cham, Switzerland: Springer, 2020, pp. 29–69.

[29] C. D. Santina, "The soft inverted pendulum with affine curvature," in *Proc. 59th IEEE Conf. Decis. Control (CDC)*, 2020, pp. 4135–4142.

[30] J. Jiang and A. Astolfi, "Stabilization of a class of underactuated nonlinear systems via underactuated back-stepping," *IEEE Trans. Autom. Control*, vol. 66, no. 11, pp. 5429–5435, Nov. 2021.

[31] N. Li, X. Liu, C. Liu, W. He, and H. Wang, "Adaptive stabilization control for a class of non-strict feedback underactuated nonlinear systems by backstepping," *IEEE Trans. Autom. Sci. Eng.*, early access, Apr. 29, 2024, doi: 10.1109/TASE.2024.3392877.

[32] R. Seifried, "Integrated mechanical and control design of underactuated multibody systems," *Nonlinear Dyn.*, vol. 67, pp. 1539–1557, Jan. 2012.

[33] G. O. Guardabassi and S. M. Savaresi, "Approximate linearization via feedback—An overview," *Automatica*, vol. 37, no. 1, pp. 1–15, 2001.

[34] C. J. Tomlin and S. S. Sastry, "Switching through singularities," *Syst. Control Lett.*, vol. 35, no. 3, pp. 145–154, 1998.

[35] K. Guemghar, B. Srinivasan, and D. Bonvin, "Approximate input-output linearization of nonlinear systems using the observability normal form," in *Proc. Eur. Control Conf. (ECC)*, 2003, pp. 713–718.

[36] J. Hauser, S. Sastry, and P. Kokotovic, "Nonlinear control via approximate input-output linearization: The ball and beam example," *IEEE Trans. Autom. Control*, vol. 37, no. 3, pp. 392–398, Mar. 1992.

[37] J. Bettega, D. Richiedei, I. Tamellin, and A. Trevisani, "Stable inverse dynamics for feedforward control of nonminimum-phase underactuated systems," *J. Mech. Robot.*, vol. 15, no. 3, 2023, Art. no. 31002.

[38] L. Ye and Q. Zong, "Tracking control of an underactuated ship by modified dynamic inversion," *ISA Trans.*, vol. 83, pp. 100–106, Dec. 2018.

[39] T. Shimizu, M. Sasaki, and T. Okada, "Tip position control of a two links flexible manipulator based on the dynamic extension technique," in *Proc. SICE Annu. Conf.*, 2007, pp. 868–873.

[40] A. De Luca and P. Lucibello, "A general algorithm for dynamic feedback linearization of robots with elastic joints," in *Proc. IEEE Int. Conf. Robot. Autom. (CAT)*, 1998, pp. 504–510.

[41] L. Ovalle, H. Ríos, M. Llama, and L. Fridman, "Continuous sliding-mode output-feedback control for stabilization of a class of underactuated systems," *IEEE Trans. Autom. Control*, vol. 67, no. 2, pp. 986–992, Feb. 2022.

[42] K. Rsetam, Z. Cao, and Z. Man, "Design of robust terminal sliding mode control for underactuated flexible joint robot," *IEEE Trans. Syst., Man, Cybern., Syst.*, vol. 52, no. 7, pp. 4272–4285, Jul. 2022.

[43] C. Urrea, J. Kern, and E. Álvarez, "Design of a generalized dynamic model and a trajectory control and position strategy for n-link underactuated revolute planar robots," *Control Eng. Pract.*, vol. 128, Nov. 2022, Art. no. 105316.

[44] S. Zoboli, S. Janny, and M. Giaccagli, "Deep learning-based output tracking via regulation and contraction theory," *IFAC-PapersOnLine*, vol. 56, no. 2, pp. 8111–8116, 2023.

[45] A. Sultangazin, L. Pannocchi, L. Fraile, and P. Tabuada, "Learning to control known feedback linearizable systems from demonstrations," *IEEE Trans. Autom. Control*, vol. 69, no. 1, pp. 189–201, Jan. 2024.

[46] C. D. Santina, R. K. Katzschmann, A. Bicchi, and D. Rus, "Dynamic control of soft robots interacting with the environment," in *Proc. IEEE Int. Conf. Soft Robot. (RoboSoft)*, 2018, pp. 46–53.

[47] D. Caradonna, M. Pierallini, C. D. Santina, F. Angelini, and A. Bicchi, "Model and control of r-soft inverted pendulum," *IEEE Robot. Autom. Lett.*, vol. 9, no. 6, pp. 5102–5109, Jun. 2024.

[48] A. Isidori, "Elementary theory of nonlinear feedback for multi-input multi-output systems," in *Nonlinear Control Systems*. London, U.K.: Springer, 1995, pp. 219–291.

[49] S. Echeandia and P. M. Wensing, "Numerical methods to compute the coriolis matrix and Christoffel symbols for rigid-body systems," *J. Comput. Nonlinear Dyn.*, vol. 16, no. 9, 2021, Art. no. 91004.

[50] F. Bullo, N. E. Leonard, and A. D. Lewis, "Controllability and motion algorithms for underactuated lagrangian systems on lie groups," *IEEE Trans. Autom. Control*, vol. 45, no. 8, pp. 1437–1454, Aug. 2000.

[51] A. De Luca and S. Iannitti, "A simple STLC test for mechanical systems underactuated by one control," in *Proc. IEEE Int. Conf. Robot. Autom. (CAT)*, 2002, pp. 1735–1740.

[52] *Controllability For Underactuated Compliant Arms*, Zenodo, Honolulu, HI, USA, Oct. 2021.

[53] L. R. Hunt and R. Su, "Control of nonlinear time-varying systems," in *Proc. 20th IEEE Conf. Decision Control Includ. Symp. Adapt. Process.*, 1981, pp. 558–563.

[54] A. Isidori, *Nonlinear Control Systems Design 1989: Selected Papers From the IFAC Symposium, Capri, Italy, 14-16 June 1989*. Amsterdam, The Netherlands: Elsevier, 2014.
[55] H. K. Khalil, *Nonlinear Control*, vol. 406. New York, NY, USA: Pearson, 2015.
[56] M. Pierallini, F. Angelini, R. Mengacci, A. Palleschi, A. Bicchi, and M. Garabini, "Trajectory tracking of a one-link flexible arm via iterative learning control," in *Proc. IEEE/RSJ Int. Conf. Intell. Robots Syst. (IROS)*, 2020, pp. 7579–7586.
[57] H. Guang, S. Bazzi, D. Sternad, and N. Hogan, "Dynamic primitives in human manipulation of non-rigid objects," in *Proc. Int. Conf. Robot. Autom. (ICRA)*, 2019, pp. 3783–3789.
[58] P. Tomei, "A simple pd controller for robots with elastic joints," *IEEE Trans. Autom. Control*, vol. 36, no. 10, pp. 1208–1213, Oct. 1991.
[59] R. Mengacci, F. Angelini, M. G. Catalano, G. Grioli, A. Bicchi, and M. Garabini, "On the motion/stiffness decoupling property of articulated soft robots with application to model-free torque iterative learning control," *Int. J. Robot. Res.*, vol. 40, no. 1, pp. 348–374, 2021.
[60] S. P. Chhatoi, M. Pierallini, F. Angelini, C. Mastalli, and M. Garabini, "Optimal control for articulated soft robots," *IEEE Trans. Robot.*, vol. 39, no. 5, pp. 3671–3685, Oct. 2023.

Michele Pierallini (Member, IEEE) received the B.S. degree in biomedical engineering and the M.S. degree (*cum laude*) in automation and robotics engineering from the University of Pisa, Pisa, Italy, in 2017 and 2020, respectively, where he is currently pursuing the Ph.D. degree in robotics with the Research Center Enrico Piaggio.

His current research focuses on the planning and control for soft robotic systems and learning control.

Franco Angelini (Member, IEEE) received the B.S. degree in computer engineering, the M.S. degree (*cum laude*) in automation and robotics engineering, and the Ph.D. degree (cum laude) in robotics from the University of Pisa, Pisa, Italy, in 2013, 2016, and 2020, respectively.

He is currently an Assistant Professor with the University of Pisa. His main research interests are control of soft robotic systems, grasping, and impedance planning.

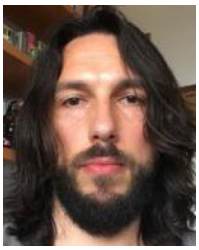

Manolo Garabini received the graduation degree in mechanical engineering and the Ph.D. degree in robotics from the University of Pisa, Pisa, Italy, in 2010 and 2014, respectively.

He is currently a Professor with the University of Pisa. He is currently the Principal Investigator with the THING H2020 EU Research Project for the University of Pisa, and the Coordinator of the Dysturbance H2020 Eurobench Subproject. Finally, he is the Coordinator of the H2020 EU Research Project Natural Intelligence. His main research interests include the design, planning, and control of soft adaptive robots.

Open Access funding provided by 'Università di Pisa' within the CRUI CARE Agreement